

Fast Successive-Cancellation List Flip Decoding of Polar Codes

Nghia Doan, Seyyed Ali Hashemi, Warren J. Gross

Abstract—This work presents a fast successive-cancellation list flip (Fast-SCLF) decoding algorithm for polar codes that addresses the high latency issue associated with the successive-cancellation list flip (SCLF) decoding algorithm. We first propose a bit-flipping strategy tailored to the state-of-the-art fast successive-cancellation list (FSCL) decoding that avoids tree-traversal in the binary tree representation of SCLF, thus reducing the latency of the decoding process. We then derive a parameterized path-selection error model to accurately estimate the bit index at which the correct decoding path is eliminated from the initial FSCL decoding. The trainable parameter is optimized online based on an efficient supervised learning framework. Simulation results show that for a polar code of length 512 with 256 information bits, with similar error-correction performance and memory consumption, the proposed Fast-SCLF decoder reduces up to 73.4% of the average decoding latency of the SCLF decoder with the same list size at the frame error rate of 10^{-4} , while incurring a maximum computational overhead of 36.2%. For the same polar code of length 512 with 256 information bits and at practical signal-to-noise ratios, the proposed decoder with list size 4 reduces 89.1% and 43.7% of the average complexity and decoding latency of the FSCL decoder with list size 32 (FSCL-32), respectively, while also reducing 83.3% of the memory consumption of FSCL-32. The significant improvements of the proposed decoder come at the cost of only 0.07 dB error-correction performance degradation compared with FSCL-32.

Index Terms—5G, polar codes, list decoding, bit flipping, machine learning.

I. INTRODUCTION

Polar codes are the first class of error-correcting codes that is proven to achieve the channel capacity of any binary symmetric channel under the low-complexity successive-cancellation (SC) decoding algorithm [1]. Recently, polar codes are selected for use in the enhanced mobile broadband (eMBB) control channel of the fifth generation of cellular communications (5G) standard, where codes with short to moderate block lengths are used [2]. The error-correction performance of short to moderate-length polar codes under SC decoding does not satisfy the requirements of the 5G standard. SC list (SCL) decoding was introduced in [3]–[5] to improve the error-correction performance of SC decoding by keeping a list of candidate message words at each decoding step. In addition, it was observed that under SCL decoding, the error-correction performance is significantly improved when the polar code is concatenated with a cyclic redundancy check (CRC) [3], [4]. Furthermore, SC-based decoding of polar code can be represented as a binary tree traversing problem [6] and it was shown that the decoders in [1], [3]–[5] experience a high decoding latency as they require a full binary tree traversal. Several fast decoding techniques were introduced

to improve the decoding latency of the conventional SC and SCL decoding algorithms [7]–[11]. The decoding operations of special constituent codes under the fast SCL (FSCL) decoding algorithms proposed in [8]–[11] can be carried out at the parent node level, thus reducing the decoding latency caused by the tree traversal.

As the memory requirement of SCL decoding grows linearly with the list size [12], it is of great interest to improve the decoding performance of SCL decoding with a small list size. To address this issue, various bit-flipping algorithms of the SCL decoder were proposed to significantly improve the error-correction performance of SCL decoding with the same list size [13], [14]. In [13], given that the initial SCL decoding attempt does not satisfy the CRC verification, the authors proposed an algorithm that flips the first erroneous bit of the best decoding path in the next decoding attempt and the error position is estimated using a correlation matrix. On the other hand, the authors in [14] estimate the bit index at which the correct path is discarded from the initial SCL decoding, then in the next decoding attempt all the paths that were discarded at the estimated error position are selected to continue the decoding. It was observed that the decoder in [14] provides a better error-correction performance when compared with the decoder proposed in [13]. In addition, the estimation of the error bit in [13] requires costly matrix multiplication operations whose complexity scales with the number of information bits. However, the decoders introduced in [13], [14] also fully traverses the polar code decoding tree as required by SCL decoding, thus resulting in a high decoding latency.

In this paper, a fast SCLF (Fast-SCLF) decoding algorithm is proposed to tackle the underlying high-decoding latency of the SCL flip (SCLF) decoder introduced in [14]. In particular, a bit-flipping strategy tailored to FSCL decoding of polar codes is first introduced. Then, a path-selection error metric is derived for the proposed bit-flipping strategy. The proposed path-selection error metric utilizes a trainable parameter to improve the estimation accuracy of the error position, which is optimized online using an efficient supervised learning framework. By utilizing online training, the proposed path-selection error-model does not require the parameter to be optimized offline at various signal-to-noise ratios (SNRs). Instead, the parameter is automatically optimized at the operating SNR of the decoder, which obviates the need for pilot signals. Our simulation results illustrate that for a polar code of length 512 with 256 information bits at the frame error rate of 10^{-4} , with similar error-correction performance and memory consumption, the proposed Fast-SCLF decoder reduces up to 73.4%

of the average decoding latency of the SCLF decoder with the same list size, while incurring a maximum computational overhead of 36.2%. For the same polar code of length 512 with 256 information bits and at practical SNR values, the proposed decoder with list size 4 reduces 89.1% and 43.7% of the average complexity and decoding latency of the FSCL decoder with list size 32 (FSCL-32), respectively, while also reducing 83.3% of the memory consumption of FSCL-32. Note that the significant complexity reductions only come at the cost of 0.07 dB error-correction performance degradation.

The remainder of this paper is organized as follows. Section II provides the background on polar codes and their decoding algorithms. Section III proposes the Fast-SCLF decoding algorithm. The simulation results are reported in Section IV, followed by concluding remarks drawn in Section V.

II. PRELIMINARIES

We start this section by first introducing notations. Throughout this paper boldface letters indicate vectors and matrices, while unless otherwise specified non-boldface letters indicate either binary, integer or real numbers. In addition, we also denote $\mathbf{a}_{i_{\min}^{i_{\max}}} = \{a_{i_{\min}}, \dots, a_{i_{\max}}\}$ as a vector of size $i_{\max} - i_{\min} + 1$ containing the a elements from index i_{\min} to i_{\max} , where $i_{\min} < i_{\max}$. Sets are denoted by blackboard bold letters, e.g., \mathbb{R} is the set containing real numbers. Finally, $\mathbb{1}_X$ is an indicator function where $\mathbb{1}_X = 1$ if the event X is true, and $\mathbb{1}_X = 0$ otherwise.

A. Polar Encoding

A polar code $\mathcal{P}(N, K)$ of length N with K information bits is constructed by applying a linear transformation to the binary message word $\mathbf{u} = \{u_1, \dots, u_N\}$ as $\mathbf{x} = \mathbf{u}\mathbf{G}^{\otimes n}$ where $\mathbf{x} = \{x_1, \dots, x_N\}$ is the codeword, $\mathbf{G}^{\otimes m}$ is the n -th Kronecker power of the polarizing matrix $\mathbf{G} = \begin{bmatrix} 1 & 0 \\ 1 & 1 \end{bmatrix}$, and $n = \log_2 N$. The vector \mathbf{u} contains a set \mathbb{I} of K information bit indices and a set \mathbb{I}^c of $N - K$ frozen bit indices, with \mathbb{I} and \mathbb{I}^c are both known to the encoder and the decoder. The values of all the frozen bits are set to 0. The codeword \mathbf{x} is then modulated and sent through the channel. In this paper, binary phase-shift keying (BPSK) modulation and additive white Gaussian noise (AWGN) channel model are considered. Therefore, the soft vector of the transmitted codeword received by the decoder is given as $\mathbf{y} = (\mathbf{1} - 2\mathbf{x}) + \mathbf{z}$, where $\mathbf{1}$ is an all-one vector of size N , and \mathbf{z} is a Gaussian noise vector of size N with variance σ^2 and zero mean. In the log-likelihood ratio (LLR) domain, the LLR vector of the transmitted codeword is given as $\alpha_n = \ln \frac{Pr(\mathbf{x}=0|\mathbf{y})}{Pr(\mathbf{x}=1|\mathbf{y})} = \frac{2\mathbf{y}}{\sigma^2}$.

B. Successive-Cancellation and Successive-Cancellation List Decoding

An example of a factor-graph representation for $\mathcal{P}(16, 8)$ is depicted in Fig. 1(a) with the frozen set $\mathbb{I}^c = \{1, 2, 3, 4, 5, 9, 10, 11\}$. To obtain the message word under SC decoding, the soft LLR values and the hard bit estimations are propagated through all the processing elements (PEs), which are depicted in Fig. 1(b). The

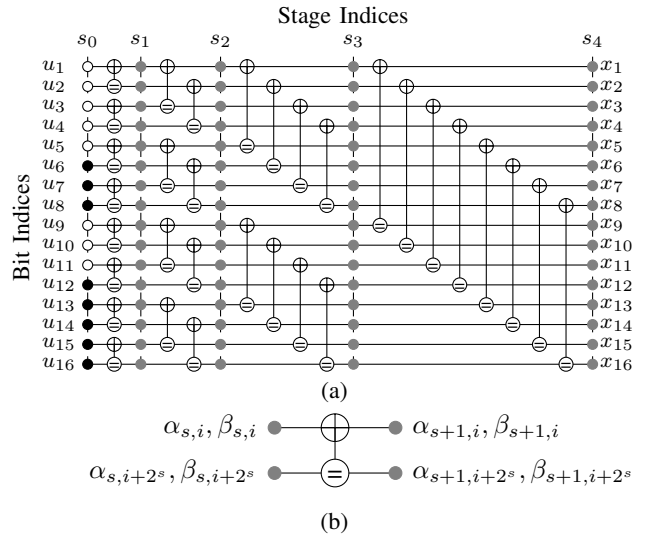


Fig. 1: (a) Factor graph representation of $\mathcal{P}(16, 8)$, and (b) a processing element (PE) of polar codes.

PE in Fig. 1(b) takes the soft LLR values $\alpha_{s+1,i}$ and $\alpha_{s+1,i+2^s}$ as inputs, and outputs the estimated hard values $\beta_{s+1,i}$ and $\beta_{s+1,i+2^s}$ by first performing the following computations: $\alpha_{s,i} = f(\alpha_{s+1,i}, \alpha_{s+1,i+2^s})$ and $\alpha_{s,i+2^s} = g(\alpha_{s+1,i}, \alpha_{s+1,i+2^s}, \beta_{s,i})$ [1]. Note that $\alpha_{s,i}$ and $\beta_{s,i}$ are the soft LLR value and the hard-bit estimation at the s -th stage and the i -th bit, respectively, and the min-sum approximation formulations of f and g are $f(a, b) = \min(|a|, |b|) \text{sgn}(a) \text{sgn}(b)$, and $g(a, b, c) = b + (1 - 2c)a$ [1]. The soft LLR values at the n -th stage are initialized to α_n and the hard-bit estimation of an information bit at the 0-th stage is obtained as $\hat{u}_i = \beta_{0,i} = \frac{1 - \text{sgn}(\alpha_{1,i})}{2}$, $\forall i \in \mathbb{I}$ [1]. Given that $\beta_{s,i}$ and $\beta_{s,i+2^s}$ are provided by other PEs or are calculated at the 0-th state, $\beta_{s+1,i}$ and $\beta_{s+1,i+2^s}$ are then computed as $\beta_{s+1,i} = \beta_{s,i} \oplus \beta_{s,i+2^s}$ and $\beta_{s+1,i+2^s} = \beta_{s,i+2^s}$ [1].

SCL decoding was introduced to significantly improve the error-correction performance of SC decoding [3]–[5]. Under SCL decoding, the estimation of an information bit \hat{u}_i ($i \in \mathbb{I}$) is considered to be both 0 and 1, causing a path splitting and doubling the number of candidate codewords (decoding paths) after each splitting. To prevent the exponential growth of the number of decoding paths, a path metric is utilized to select the L most probable decoding paths after each information bit is decoded. The path metric is obtained as [5]

$$\text{PM}_l = \begin{cases} \text{PM}_l + |\alpha_{0,i_l}| & \text{if } \hat{u}_i \neq \frac{1 - \text{sgn}(\alpha_{0,i_l})}{2}, \\ \text{PM}_l & \text{otherwise,} \end{cases} \quad (1)$$

where α_{0,i_l} denotes the soft value of the i -th bit ($1 \leq i \leq N$) at stage 0 of the l -th path ($1 \leq l \leq 2L$). Initially, $\text{PM}_l = 0$, $\forall l$. After each information bit is decoded, only L paths with the smallest path metric values, i.e., the L most-probable decoding paths, are selected from the $2L$ paths to continue the decoding. After the last information bit is decoded, only the decoding path that has the smallest path metric is selected as the decoding output.

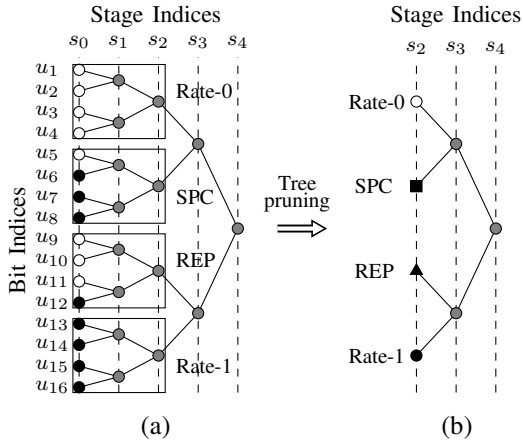


Fig. 2: (a) The full binary tree representation of $\mathcal{P}(16, 8)$ illustrated in Fig. 1(a), and (b) the pruned binary tree representation of the same polar code.

In a practical scenario such as in the 5G standard, the message word is often concatenated with a CRC of size C to allow error detection. In addition, it was observed in [3], [4] that the error-correction performance of SCL decoding is greatly improved when a CRC is concatenated to polar codes.

C. Fast Successive-Cancellation List Decoding

Fig. 2(a) shows a full binary tree representation of $\mathcal{P}(16, 8)$, whose factor graph is depicted in Fig. 1(a). The authors in [9]–[11] proposed fast decoding operations for various special nodes under SCL decoding, which preserve the error-correction performance of SCL decoding while preventing tree-traversal to the leaf nodes. Thus, the decoding latency of SCL decoding is significantly reduced. Similar to [9], we consider four types of special nodes, namely Rate-0, Rate-1, repetition (REP), and single parity check (SPC), for all the fast SCL-based decoding algorithms in this paper.

Consider a parent node ν located at the s -th stage ($0 < s \leq n$) of the polar code binary tree. There are N_ν LLR values and N_ν hard decisions associated with this node, where $N_\nu = 2^s$. Let α_{ν_l} and β_{ν_l} be the vectors containing the soft and hard values associated with a parent node ν of the l -th decoding path, respectively. α_{ν_l} and β_{ν_l} are defined as

$$\begin{cases} \alpha_{\nu_l} = \{\alpha_{s, i_{\min\nu_l}}, \dots, \alpha_{s, i_{\max\nu_l}}\}, \\ \beta_{\nu_l} = \{\beta_{s, i_{\min\nu_l}}, \dots, \beta_{s, i_{\max\nu_l}}\}, \end{cases}$$

where $i_{\min\nu_l}$ and $i_{\max\nu_l}$ are the bit indices corresponding to ν such that $1 \leq i_{\min\nu_l} < i_{\max\nu_l} \leq N$ and $i_{\max\nu_l} - i_{\min\nu_l} = N_\nu - 1$. For all the fast SCL-based decoders considered in this paper, the elements of α_{ν_l} corresponding to the SPC and Rate-1 nodes are considered to be sorted in the following order [9]:

$$|\alpha_{s, i_{\min\nu_l}^*}| \leq \dots \leq |\alpha_{s, i_{\max\nu_l}^*}|, \quad (2)$$

where $i_{\min} \leq i_{\min\nu_l}^*, i_{\max\nu_l}^* \leq i_{\max}$. In addition, let τ be the minimum number of path splittings that allows FSCL decoding to preserve the error-correction performance of the conventional SCL decoding algorithm [9]. The definitions and decoding

operations of each special node under FSCL decoding are given as follows.

1) *Rate-0 node*: All the leaf nodes of a Rate-0 node are frozen bits. Therefore, all the hard values associated with the parent node are set to 0 and the path metric of the l -th decoding path is calculated as [9]

$$PM_l = PM_l + \sum_{i=i_{\min\nu_l}^*}^{i_{\max\nu_l}^*} \frac{|\alpha_{s, i}| - \alpha_{s, i}}{2}. \quad (3)$$

2) *REP node*: All the leaf nodes of a REP node are frozen bits, except for $\beta_{0, i_{\max\nu_l}^*}$. The path metric of the l -th decoding path is calculated as [9]

$$PM_l = PM_l + \sum_{i=i_{\min\nu_l}^*}^{i_{\max\nu_l}^*} \frac{|\alpha_{s, i}| - (1 - 2\beta_{s, i_{\max\nu_l}^*})\alpha_{s, i}}{2}, \quad (4)$$

where $\beta_{s, i_{\max\nu_l}^*}$ denotes the bit estimate of the information bit of the REP node.

3) *Rate-1 node*: All the leaf nodes of a Rate-1 node are information bits. FSCL decoding performs τ path splittings, where $\tau = \min(L - 1, N_\nu)$ [9]. The path metric of the l -th decoding path for a Rate-1 node is calculated as [9]

$$PM_l = PM_l + \sum_{i=i_{\min\nu_l}^*}^{i_{\max\nu_l}^*} \frac{|\alpha_{s, i}| - (1 - 2\beta_{s, i})\alpha_{s, i}}{2}, \quad (5)$$

where $\beta_{s, i}$ denotes the bit estimate of the i -th bit of ν .

4) *SPC node*: All the leaf nodes of an SPC node are information bits, except for $\beta_{0, i_{\min\nu_l}^*}$. The parity check sum of the l -th path is first obtained as [9]

$$p_l = \bigoplus_{i=i_{\min\nu_l}^*}^{i_{\max\nu_l}^*} \frac{1 - \text{sgn}(\alpha_{s, i})}{2}. \quad (6)$$

The path metric is then updated as [9]

$$PM_l = PM_l + p_l |\alpha_{s, i_{\min\nu_l}^*}|. \quad (7)$$

The decoding continues with τ path splittings, where $\tau = \min(L, N_\nu)$ [9]. In each new path splitting, the path metric is then updated as [9]

$$PM_l = \begin{cases} PM_l + |\alpha_{s, i}| + (1 - 2p_l) |\alpha_{s, i_{\min\nu_l}^*}| & \text{if } 1 - 2\beta_{s, i} \neq \text{sgn}(\alpha_{s, i}), \\ PM_l & \text{otherwise,} \end{cases} \quad (8)$$

then the parity check sum is updated as [10]

$$p_l = \begin{cases} 1 \oplus p_l & \text{if } 1 - 2\beta_{s, i} \neq \text{sgn}(\alpha_{s, i}), \\ p_l & \text{otherwise.} \end{cases} \quad (9)$$

where $i_{\min\nu_l}^* < i \leq i_{\max\nu_l}^*$, and i is selected by following the order of the sorted absolute LLR values [9]. When all the bits are estimated, the hard decision of the least reliable bit is updated to maintain the parity check condition of the SPC node, which is given as [9]

$$\beta_{s, i_{\min\nu_l}^*} = \bigoplus_{i_{\min\nu_l}^* < i \leq i_{\max\nu_l}^*} \beta_{s, i}. \quad (10)$$

The memory requirements of SCL and FSCL decoding algorithms with list size L in terms of the number of memory bits are given as [5], [9]

$$\mathcal{M}_{\text{SCL}} = \mathcal{M}_{\text{FSCL}} = N(L+1)b_f + 2LN, \quad (11)$$

where b_f is the number of bits used to quantize a floating-point number.

D. Successive-Cancellation List Flip Decoding

SCLF decoding relies on a CRC verification to indicate whether the initial SCL decoding attempt is successful or not. If the first SCL decoding attempt does not satisfy the CRC verification, the SCLF decoding algorithm tries to identify the information bit index ι , at which the correct path is discarded from the list of the L most probable decoding paths [14]. Given that the ι -th bit index is correctly identified, in the next decoding attempt and after the path splitting occurs at the ι -th bit index, the path selection is reversed in the sense that the L decoding paths that have the highest (worst) path metrics are selected to continue the decoding [14]. This reversed path-selection scheme recovers the correct decoding path, which was discarded at the initial SCL decoding, to the list of the active decoding paths. SCLF decoding then performs conventional SCL decoding operations for all the bit indices following ι .

As we only need to locate the error decision occurred at a path splitting of an information bit, in this section the bit indices are referred to information bits and are indexed from 1 to $K+C$. Given that at the i -th information bit under SCL decoding, there are L active decoding paths denoted as l , $l \in [1, 2L]$. After the path splitting of the current L active paths, the path metrics of the new $2L$ paths are computed and sorted. Let l' be the index of a discarded decoding path after the path metric sorting, i.e., the path metric corresponding to l' is among the L largest path metric values. The probability that the path with index l' is the correct decoding path is [15]

$$Pr(\hat{\mathbf{u}}_{1_{l'}}^{i_{l'}} = \mathbf{u}_1^i | \boldsymbol{\alpha}_n) = \prod_{\substack{1 \leq j \leq i \\ \forall j \in \mathbb{A}_{l'}^c}} Pr(\hat{u}_{j_{l'}} = u_j | \boldsymbol{\alpha}_n, \hat{\mathbf{u}}_{1_{l'}}^{j_{l'}-1} = \mathbf{u}_1^{j-1}) \\ \times \prod_{\substack{1 \leq j \leq i \\ \forall j \in \mathbb{A}_{l'}^c}} \left[1 - Pr(\hat{u}_{j_{l'}} = u_j | \boldsymbol{\alpha}_n, \hat{\mathbf{u}}_{1_{l'}}^{j_{l'}-1} = \mathbf{u}_1^{j-1}) \right], \quad (12)$$

where $Pr(\hat{\mathbf{u}}_{1_{l'}}^{i_{l'}} = \mathbf{u}_1^i | \boldsymbol{\alpha}_n) = Pr(\hat{u}_{1_{l'}} = u_1, \dots, \hat{u}_{i_{l'}} = u_i | \boldsymbol{\alpha}_n)$. $\mathbb{A}_{l'}$ is the set of information bit indices where their hard decisions follow the sign of the corresponding LLR values, while $\mathbb{A}_{l'}^c$ is the set of information bit indices whose hard decisions do not follow the sign of the LLR values [14].

Note that $Pr(\hat{u}_{j_{l'}} = u_j | \boldsymbol{\alpha}_n, \hat{\mathbf{u}}_{1_{l'}}^{j_{l'}-1} = \mathbf{u}_1^{j-1})$ is not available during the course of decoding as \mathbf{u} is unknown, thus it is approximated as [14], [15]

$$Pr(\hat{u}_{j_{l'}} = u_j | \boldsymbol{\alpha}_n, \hat{\mathbf{u}}_{1_{l'}}^{j_{l'}-1} = \mathbf{u}_1^{j-1}) \approx \frac{1}{1 + \exp(-\lambda |\alpha_{0,j_{l'}}|)}, \quad (13)$$

where $\lambda \in \mathbb{R}^+$ is a perturbation parameter that is optimized offline to improve the approximation accuracy of (13).

The probability that the correct decoding path is discarded at the information bit with index i is [14]

$$P_i = \sum_{\forall l'} Pr(\hat{\mathbf{u}}_{1_{l'}}^{i_{l'}} = \mathbf{u}_1^i | \boldsymbol{\alpha}_n). \quad (14)$$

Therefore, the bit index at which the error decision is most likely to take place is [14]

$$\iota = \arg \max_{\log_2 L < i \leq K+C} P_i. \quad (15)$$

Directly computing (14) is not numerically stable [14], [15]. Thus, a flipping metric based on the max-log approximation is derived from (14) as [14]

$$Q_i = -\frac{1}{\lambda} \ln P_i \approx -\max_{\forall l'} \left[\frac{1}{\lambda} \ln Pr(\hat{\mathbf{u}}_{1_{l'}}^{i_{l'}} = \mathbf{u}_1^i | \boldsymbol{\alpha}_n) \right] \\ \approx \min_{\forall l'} \left[\sum_{\forall j \in \mathbb{A}_{l'}^c} |\alpha_{0,j_{l'}}| + \sum_{1 \leq j \leq i} \frac{1}{\lambda} \ln [1 + \exp(-\lambda |\alpha_{0,j_{l'}}|)] \right]. \quad (16)$$

The computation of Q_i can be further simplified by using a hardware-friendly approximation introduced in [16]:

$$f_\lambda(x) = \frac{1}{\lambda} \ln [1 + \exp(-\lambda|x|)] \approx \begin{cases} a_\lambda & \text{if } |x| \leq b_\lambda, \\ 0 & \text{otherwise,} \end{cases} \quad (17)$$

where $a_\lambda, b_\lambda \in \mathbb{R}^+$ are tunable parameters selected based on a predetermined value of λ . However, this approach requires the optimizations of the parameters $\{\lambda, a_\lambda, b_\lambda\}$. On the other hand, in [17] the authors approximate the term $Pr(\hat{u}_{j_{l'}} = u_j | \boldsymbol{\alpha}_n, \hat{\mathbf{u}}_{1_{l'}}^{j_{l'}-1} = \mathbf{u}_1^{j-1})$ in (13) as

$$Pr(\hat{u}_{j_{l'}} = u_j | \boldsymbol{\alpha}_n, \hat{\mathbf{u}}_{1_{l'}}^{j_{l'}-1} = \mathbf{u}_1^{j-1}) \approx \frac{1}{1 + \exp(\theta - |\alpha_{0,j_{l'}}|)}, \quad (18)$$

where similar to λ , $\theta \in \mathbb{R}^+$ is an additive perturbation parameter used to improve the approximation accuracy. The flipping metric Q_i under the approximation provided in (18) is then given as [14], [17]

$$Q_i = -\ln P_i \approx -\max_{\forall l'} \left[\ln Pr(\hat{\mathbf{u}}_{1_{l'}}^{i_{l'}} = \mathbf{u}_1^i | \boldsymbol{\alpha}_n) \right] \\ \approx \min_{\forall l'} \left[\sum_{\forall j \in \mathbb{A}_{l'}^c} (|\alpha_{0,j_{l'}}| - \theta) + \sum_{1 \leq j \leq i} \text{ReLU}(\theta - |\alpha_{0,j_{l'}}|) \right], \quad (19)$$

where $\text{ReLU}(a) = a$ if $a \geq 0$ and $\text{ReLU}(a) = 0$ if $a < 0$. Thus, the most probable information bit index where the correct path is discarded can be estimated as

$$\iota = \arg \min_{\log_2 L < i \leq K+C} Q_i. \quad (20)$$

In this paper, we implement the hardware-friendly SCLF decoder using (19) as it only requires the optimization of θ .

III. FAST SUCCESSIVE-CANCELLATION LIST FLIP DECODING

A. Bit-flipping Scheme for FSCL Decoding

We first introduce the bit-flipping scheme tailored to FSCL decoding by illustrating the proposed scheme under various examples. We consider the case where an all-zero codeword of $\mathcal{P}(16, 8)$ is transmitted through the channel, whose binary-tree representation is depicted in Fig. 2(a). Similar to SCL-based decoding, under FSCL-based decoding, we denote by l the path index of the active decoding paths, while \tilde{l} is used to indicate the indices of the paths that are forked from the current L active decoding paths indexed by l . Finally, \tilde{l} indicates the path indices of the decoding paths that are discarded due to their high path metric values, and $l, \tilde{l}, l' \in [1, 2L]$.

1) *Bit-Flipping Scheme for SPC Nodes*: Fig. 3 shows an example of FSCL decoding when applied to the SPC node of $\mathcal{P}(16, 8)$ with $L = 2$. The decoding order is first determined by sorting the magnitude LLR values associated with the SPC node in the increasing order. In this example, the following decoding order is considered: $\{\beta_{2,8_1}, \beta_{2,5_1}, \beta_{2,7_1}, \beta_{2,6_1}\}$, thus $\beta_{2,8_1}$ is selected as the parity bit of the SPC node for all the active decoding paths, and the path splitting occurred at $\beta_{2,7_1}$ is considered in this example. The path with indices $\tilde{l} \in \{2, 3\}$ are forked from the paths with indices $l \in \{0, 1\}$, followed by the path metric sorting operations. The most probable decoding paths with indices $l = \{0, 1\}$, i.e., $\{\beta_{2,8_0}, \beta_{2,5_0} = 1, \beta_{2,7_0} = 1, \beta_{2,6_0}\}$ and $\{\beta_{2,8_1}, \beta_{2,5_1} = 0, \beta_{2,7_1} = 1, \beta_{2,6_1}\}$, respectively, are then selected to continue the decoding, while the paths with indices $l' \in \{2, 3\}$ are discarded as illustrated in Fig. 3.

Note that, at this stage the parity bit $\beta_{2,8_1}$ and the last bit $\beta_{2,6_1}$ of the SPC node are not yet decoded. As an all-zero codeword is sent, it can be observed that the correct decoding path is $l' = 3$ which is discarded after $\beta_{2,7_1}$ is decoded, i.e., after the second path splitting under FSCL decoding. Therefore, this erroneous path selection decision should be reversed in the next decoding attempt by swapping the path indices of l' and l after the second path splitting, given that the erroneous decision occurred in the initial SCL decoding can

Node type	Path splitting index	$l' = 2$	$l' = 3$
SPC	0	$\beta_{2,8_2} = \text{n/a}$	$\beta_{2,8_3} = \text{n/a}$
	1	$\beta_{2,5_2} = 1$	$\beta_{2,5_3} = 0$
	2	$\beta_{2,7_2} = 0$	$\beta_{2,7_3} = 0$
	3	$\beta_{2,6_2} = \text{n/a}$	$\beta_{2,6_3} = \text{n/a}$

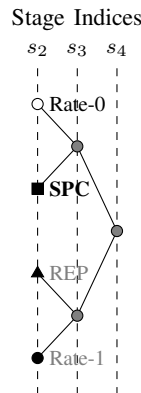


Fig. 3: An example of FSCL decoding applied to an SPC node of size 4 with $L = 2$, where the decoding is at the second path splitting. $l' \in \{2, 3\}$ are the indices of the discarded paths.

be detected by a CRC verification. In addition, the bit-flipping operation is not applicable for the parity bits of the SPC nodes, since the values of the parity bits are computed after the values of all the other bits are determined to satisfy the parity check constraint (see (10)). Therefore, if all the other bits of the SPC node are correctly decoded, the parity bit of this decoding path is also correctly decoded. As a result, the proposed algorithm only considers $N_\nu - 1$ possibilities to identify a bit flip that occurs in an SPC node. This is significantly smaller than the maximum search space of size $\binom{N_\nu}{2}$ required to flip a pair of indices to maintain the parity check constrain as used in [16], especially as N_ν increases.

In this example, the minimum number of path splittings required by the SPC node to preserve the SCL performance is $\tau = \min\{L, N_\nu\} = \min\{2, 4\} = 2$, where ν is the sized-4 SPC node. Thus, there is no need to perform a path splitting for $\beta_{2,6_1}$ as $\beta_{2,6_1}$ is set to follow the sign of its LLR value [9]. However, if an error decision is occurred at the decoding of $\beta_{2,6_1}$ (or in general at a bit index after the τ path splittings), in the next decoding attempt the hard values at the estimated error position are simply flipped for all the active paths. The path metrics of the active paths are then updated by adding with the magnitude LLR values corresponding to the flipped hard estimates.

2) *Bit-Flipping Scheme for REP Nodes*: Since the soft and hard estimate of the information bit associated with a REP node can be directly obtained at the parent node level under FSCL decoding, the path splitting operation under FSCL decoding applied to the information bit of a REP node is similar to that of SCL decoding when applied to an information bit at the leaf node level. Therefore, in this paper, the reversed path selection scheme used in SCLF decoding is directly applied to the information bit associated with a REP node or to an information bit at the leaf-node level under FSCL decoding, given that the erroneous decision is estimated to take place at this information bit.

3) *Bit-Flipping Scheme for Rate-1 Nodes*: Fig. 4 shows an example of FSCL decoding applied to the Rate-1 node of

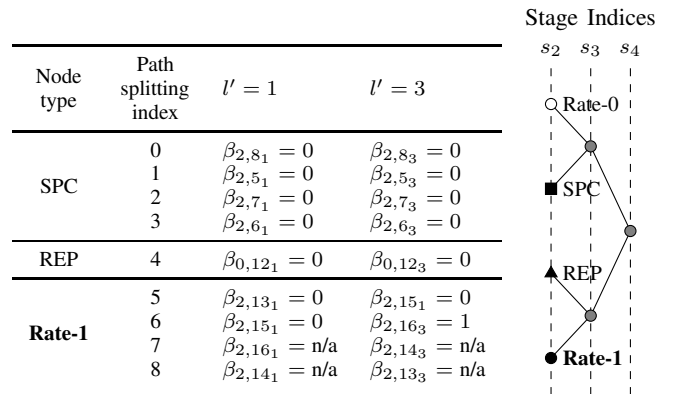


Fig. 4: An example of FSCL decoding applied to a Rate-1 node of size 4 with $L = 2$, where the decoding is at the 6-th path splitting. $l' \in \{1, 3\}$ are the indices of the discarded paths.

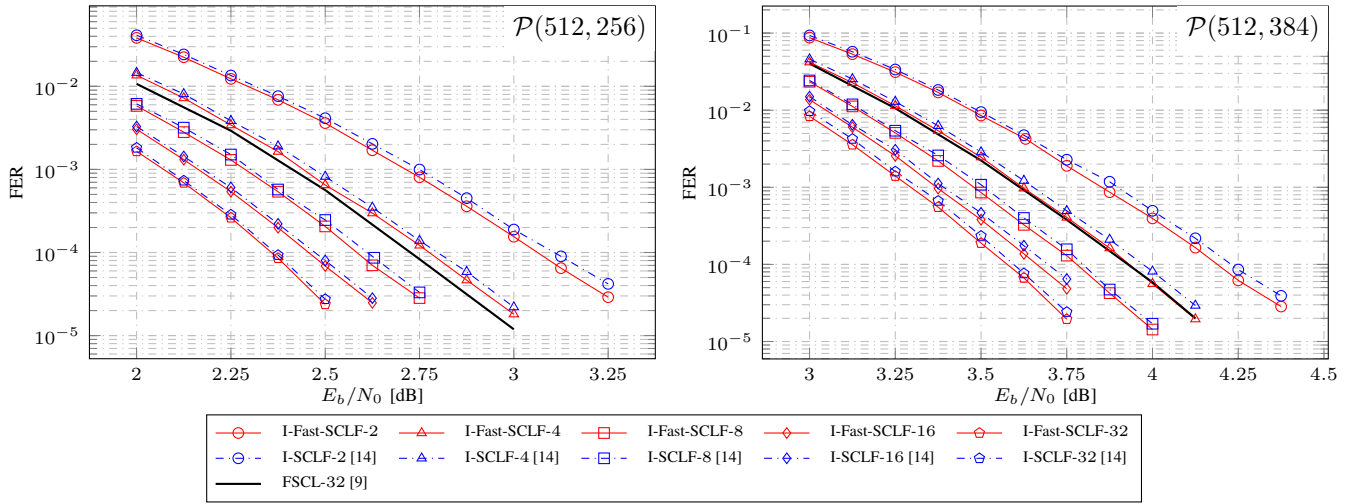


Fig. 5: Ideal error-correction performance in terms of FER of the proposed Fast-SCLF decoder. The FER values of the ideal SCLF and FSCL decoders are also plotted for comparison.

$\mathcal{P}(16, 8)$ after the 6-th path splitting with $L = 2$. In Fig. 4, the hard estimates of the two discarded paths with indices $l' \in \{1, 3\}$ are indicated, while the hard estimates of the surviving paths with indices $l \in \{0, 2\}$ are omitted. It can be observed that the decoding path with index $l' = 1$ is the correct path as all the estimated bits are 0, which is discarded after the bit $\beta_{2,15_1}$ is decoded. Therefore, in the next decoding attempt, the decoding paths with indices $l' \in \{1, 3\}$ will be selected to continue the decoding instead of the paths with indices $l \in \{0, 2\}$. Similar to the case of an SPC node, after the minimum τ path splittings in the initial FSCL decoding, if the hard decision obtained for a bit of the Rate-1 node results in an elimination of the correct path, this erroneous decision can be reversed in the next FSCL decoding attempt by flipping the hard estimates of all the active paths at that erroneous index, followed by the path metric updates associated with the bit flips.

Fig 5 shows the ideal frame error rate (FER) of the proposed bit-flipping strategy applied to FSCL decoding for $\mathcal{P}(512, 256)$ and $\mathcal{P}(512, 384)$ with a 24-bit CRC used in $5G^1$. Note that the positions of the erroneous decoding decisions are always correctly defined by comparing the discarded paths with the correct path obtained from the sent codeword after each path splitting. Similar to SCLF decoding, the proposed scheme only aims at correcting the first erroneous decision occurred at the initial FSCL decoding attempt. We also plot the FER performance of the ideal SCLF decoding [14] and that of the FSCL decoder with list size 32 [9] for comparison. In Fig 5, the ideal SCLF and Fast-SCLF decoders with list size L are denoted as I-SCLF- L and I-Fast-SCLF- L , respectively, with $L \in \{2, 4, 8, 16, 32\}$, and the FSCL decoder with list size 32 is denoted as FSCL-32. It can be observed that the FER performance of the I-Fast-SCLF- L decoder is slightly better than that of the I-SCLF- L decoder. This is because we observed in many cases that correcting a wrong decoding decision at the parent-node level of the Rate-1 and SPC nodes

can result in the corrections of more than one information bits at the leaf-node level, resulting in a slight improvement in the FER performance of the I-Fast-SCLF- L decoder over the I-SCLF- L decoder. In the next section, a path-selection error model is derived to accurately estimate the index of the path splitting that causes the elimination of the correct path at the initial FSCL decoding. Therefore, the error-correction performance of the I-Fast-SCLF- L decoder provided in Fig. 5 serves as the empirical lower bounds of the proposed decoding algorithm.

B. Path-Selection Error Model for FSCL Decoding

We use the methods introduced in [14], [15] to estimate the erroneous path-splitting index, which predicts the error position using the LLR values associated with each discarded decoding path. Thus, the proposed path-selection error model relies on the construction of the LLR vectors obtained at each path splitting.

Consider that the first FSCL decoding attempt does not pass the CRC verification and ν is a node located at the s -th stage of the binary tree, that is visited by FSCL decoding. Let $k \in [1, K + C]$ be the path-splitting index that occurs during the decoding of ν . Let $\gamma_{l'} = \gamma_{1_{l'}}^{k_{l'}}$ be an LLR vector of a discarded decoding path l' , which contains k LLR values corresponding to the hard estimates of the discarded path l' . $\gamma_{l'}$ is constructed progressively after each information bit is decoded following the FSCL decoding schedule and up to the k -th path splitting. Formally, $\gamma_{l'}$ is obtained using the following procedure:

- If ν is a leaf node that contains an information bit:

$$\gamma_{l'} = \text{concat}(\gamma_{l'}, \alpha_{0, i_{\min_{\nu, l'}}}). \quad (21)$$

- If ν is a REP node:

$$\gamma_{l'} = \text{concat}(\gamma_{l'}, \sum_{j=i_{\min_{\nu, l'}}}^{i_{\max_{\nu, l'}}} \alpha_{s, j}). \quad (22)$$

¹In this paper we use the 24-bit CRC specified as 24C.

- If ν is a Rate-1 node: Updating $\gamma_{l'}$ using the following function after each path splitting at the j -th bit

$$\gamma_{l'} = \text{concat}(\gamma_{l'}, \alpha_{s,j}), \quad (23)$$

where $i_{\min_{\nu_{l'}}}^* \leq j \leq i_{\max_{\nu_{l'}}}^*$.

- If ν is an SPC node: Updating $\gamma_{l'}$ using the following function after each path splitting at the j -th bit

$$\gamma_{l'} = \text{concat}(\gamma_{l'}, \alpha_{s,j}), \quad (24)$$

where $i_{\min_{\nu_{l'}}}^* < j \leq i_{\max_{\nu_{l'}}}^*$. Recall that $i_{\min_{\nu_{l'}}}^*$ is the bit index of the parity bit whose LLR value is ignored when constructing $\gamma_{l'}$.

Note that $\text{concat}(\gamma_{l'}, a)$ is a function that concatenates $a \in \mathbb{R}$ to the end of $\gamma_{l'}$ and initially $\gamma_{l'} = \emptyset$. In addition, $\gamma_{l'}$ is not altered if ν does not satisfy any of the above conditions. For example, the LLR vector $\gamma_{l'}$ obtained after the 6-th path splitting in Fig. 4 for $l' = 1$ is $\gamma_{l'} = \gamma_{1_1}^{6_1} = \{\alpha_{2,5_1}, \alpha_{2,7_1}, \alpha_{2,6_1}, \alpha_{0,12_1}, \alpha_{2,14_1}, \alpha_{2,16_1}\}$. We now define the hard estimates of $\gamma_{l'}$ as $\hat{\eta}_{l'} = \hat{\eta}_{1_{l'}}^{k_{l'}}$, and the correct hard values associated with $\gamma_{l'}$ as $\eta_{l'} = \eta_{1_{l'}}^{k_{l'}}$. For instance $\hat{\eta}_{l'} = \hat{\eta}_{1_1}^{6_1} = \{\beta_{2,5_1}, \beta_{2,7_1}, \beta_{2,6_1}, \beta_{0,12_1}, \beta_{2,14_1}, \beta_{2,16_1}\}$ is the discarded decoding path obtained after the 6-th path split in Fig. 4 with $l' = 1$, and $\eta_{l'} = \eta_{1_1}^{6_1} = \{0, 0, 0, 0, 0, 0\}$.

Unlike SCLF decoding, at the same path-splitting index the hard estimates and LLR values of $\hat{\eta}_{l'}$ and $\gamma_{l'}$ of different path indices l' can correspond to different bit indices of the polar binary tree. However, similar to SCLF decoding, each instance of the hard estimates and LLR values of $\hat{\eta}_{l'}$ and $\gamma_{l'}$ are obtained sequentially by following the course of FSCL decoding, thus in this paper we utilize the conditional error probability model introduced in [14], [15] to estimate the erroneous decision occurred at the k -th path splitting of FSCL decoding. Specifically, the probability that the discarded path l' at the k -th path splitting under FSCL decoding is the correct path is

$$\begin{aligned} & Pr(\hat{\eta}_{1_{l'}}^{k_{l'}} = \eta_{1_{l'}}^{k_{l'}} | \alpha_n) \\ &= \prod_{\substack{1 \leq j \leq k \\ \forall j \in \mathbb{A}_{l'}}} Pr(\hat{\eta}_{j_{l'}} = \eta_{j_{l'}} | \alpha_n, \hat{\eta}_{1_{l'}}^{j_{l'}-1} = \eta_{1_{l'}}^{j_{l'}-1}) \\ &\times \prod_{\substack{1 \leq j \leq k \\ \forall j \in \mathbb{A}_{l'}^c}} \left[1 - Pr(\hat{\eta}_{j_{l'}} = \eta_{j_{l'}} | \alpha_n, \hat{\eta}_{1_{l'}}^{j_{l'}-1} = \eta_{1_{l'}}^{j_{l'}-1}) \right], \end{aligned} \quad (25)$$

where $\mathbb{A}_{l'}$ is the set of bit indices j in which the hard estimates $\hat{\eta}_{j_{l'}}$ follow the sign of $\gamma_{j_{l'}}$, and $\mathbb{A}_{l'}^c$ is the set of bit indices j in which the hard estimates $\hat{\eta}_{j_{l'}}$ do not follow the sign of $\gamma_{j_{l'}}$. Similar to \mathbf{u} , $\eta_{l'}$ is also not available during the decoding process, thus we use the approximation introduced in [17] to estimate the unknown probability $Pr(\hat{\eta}_{j_{l'}} = \eta_{j_{l'}} | \alpha_n, \hat{\eta}_{1_{l'}}^{j_{l'}-1} = \eta_{1_{l'}}^{j_{l'}-1})$ as

$$Pr(\hat{\eta}_{j_{l'}} = \eta_{j_{l'}} | \alpha_n, \hat{\eta}_{1_{l'}}^{j_{l'}-1} = \eta_{1_{l'}}^{j_{l'}-1}) \approx \frac{1}{1 + \exp(\theta - |\gamma_{j_{l'}}|)}. \quad (26)$$

To enable a numerically stable implementation, a path-selection error metric obtained at the k -th path splitting based on (26) and (25) can be defined as

$$\begin{aligned} Q_k &= -\ln \left[\sum_{\forall l'} Pr(\hat{\eta}_{1_{l'}}^{k_{l'}} = \eta_{1_{l'}}^{k_{l'}} | \alpha_n) \right] \\ &\approx -\ln \left[\max_{\forall l'} Pr(\hat{\eta}_{1_{l'}}^{k_{l'}} = \eta_{1_{l'}}^{k_{l'}} | \alpha_n) \right] \\ &\approx \min_{\forall l'} \left[\sum_{\substack{1 \leq j \leq k \\ \forall j \in \mathbb{A}_{l'}^c}} (|\gamma_{j_{l'}}| - \theta) + \sum_{1 \leq j \leq k} \text{ReLU}(\theta - |\gamma_{j_{l'}}|) \right]. \end{aligned} \quad (27)$$

Consequently, the most probable erroneous position i is obtained as

$$i = \arg \min_{\log_2 L < k \leq K+C} Q_k. \quad (28)$$

The error metric described in (27) can be progressively calculated during the course of decoding, allowing for an efficient implementation of the proposed decoder. In particular, for each active decoding path l we denote by q_{k-1_l} the path-error metric at the $(k-1)$ -th path splitting of l , which is given as

$$q_{k-1_l} = \sum_{\substack{1 \leq j \leq k-1 \\ \forall j \in \mathbb{A}_l^c}} (|\gamma_{j_l}| - \theta) + \sum_{1 \leq j \leq k-1} \text{ReLU}(\theta - |\gamma_{j_l}|) \quad (29)$$

if $k > 1$ and $q_{0_l} = 0 \forall l$. The path-error metric of the path l at the k -th path splitting can be calculated from q_{k-1_l} as

$$q_{k_l} = q_{k-1_l} + \text{ReLU}(\theta - \gamma_{k_l}). \quad (30)$$

Then, the path-error metric of the forked path with index \tilde{l} originated from l , whose hard value at the k -th path splitting does not follow the sign of its LLR value, is calculated as

$$q_{k_{\tilde{l}}} = q_{k_l} + |\gamma_{k_{\tilde{l}}}| - \theta. \quad (31)$$

(30) and (31) are used to compute the path-error metrics for all the $2L$ paths associated with the current L active paths and the L forked paths progressively. Next, the path metric sorting is carried out and a list of discarded paths with indices l' is determined. The flipping metric in (27) is then given as

$$Q_k = q_{k_{l'_{\min}}}, \quad (32)$$

where $l'_{\min} = \arg \min_{l'} q_{k_{l'}}$. Therefore, under a practical implementation one only needs to maintain the path-error metrics q corresponding to the $2L$ decoding paths to progressively calculate the path-selection error metric Q_k .

In this paper, we formalize the optimization of the parameter θ as a machine learning problem and use online supervised learning to train θ . Compared to the optimization technique with Monte-Carlo simulations, supervised learning directly updates the parameters to minimize a specific loss function which results in a quick convergence to a (local) optimal of the parameter. On the other hand, under Monte-Carlo simulations, the optimization is carried out offline at various SNR values and the parameter is searched over a range of its value.

In addition, by using online training the parameter can be automatically optimized at the operating SNR of the decoder during the course of decoding, allowing the proposed decoder to be applicable for applications that do not need to estimate the channel conditions. The proposed training framework is provided as follows.

Let \mathbb{D} be a data batch that contains $|\mathbb{D}|$ instances of the path-selection error metrics $\mathbf{Q} = \mathbf{Q}_1^{K+C}$, where the corresponding message word estimated by the initial FSCL decoding algorithm does not satisfy the CRC test. Under supervised learning, we need to obtain the erroneous path-splitting index ι_e to train θ . Note that in a practical scenario, the proposed decoder often requires a maximum number of m additional FSCL decoding attempts where a different estimated error index is associated with each additional decoding attempt. By assuming that a correct codeword is obtained if the CRC verification is successful, the error index ι_e can be obtained when a secondary FSCL decoding attempt passes the CRC verification. Let \mathbf{o} be a one-hot encoded vector of size $K+C$ that indicates the error bit index ι_e as

$$o_k = \begin{cases} 1 & \text{if } k = \iota_e, \\ 0 & \text{otherwise.} \end{cases} \quad (33)$$

A data sample $d \in \mathbb{D}$ contains a pair of the input \mathbf{Q} and its corresponding encoded output \mathbf{o} , i.e., $d \triangleq \{\mathbf{Q}, \mathbf{o}\}$.

Given a data sample d , the path-selection error metric introduced in Section III-B provides an estimate of ι_e as ι by selecting the index corresponding to the smallest element of \mathbf{Q} (see (28)). To enable training, the error metrics are converted to the probability domain using the following softmax conversion:

$$\hat{o}_k = \frac{\exp(-Q_k)}{\sum_{j=1}^{K+C} \exp(-Q_j)}, \quad (34)$$

where Q_k is manually set to ∞ for $k \in [1, \log_2 L]$ as the correct decoding path is always present in the first $\log_2 L$ path splittings. It can be seen from (27) and (34) that the bit index that has the smallest error metric is also the bit index that has the highest probability to be in error. In this paper, we use the binary cross entropy (BCE) loss function to quantify the dissimilarity between the target output \mathbf{o} and the estimated output $\hat{\mathbf{o}}$ as

$$\text{Loss} = - \sum_{k=1}^{K+C} [o_k \ln \hat{o}_k + (1 - o_k) \ln(1 - \hat{o}_k)]. \quad (35)$$

The parameter θ can then be trained to minimize the loss function by using the stochastic gradient descent (SGD) technique or one of its variants. An update step is given as

$$\theta = \theta - \frac{\sigma}{|\mathbb{D}|} \sum_{\forall d \in \mathbb{D}} \frac{\partial \text{Loss}}{\partial \theta}, \quad (36)$$

where $\sigma \in \mathbb{R}^+$ is the learning rate and $\frac{1}{|\mathbb{D}|} \sum_{\forall d \in \mathbb{D}} \frac{\partial \text{Loss}}{\partial \theta}$ is the estimation of the true gradient obtained from a data set that contains an infinite number of data samples d . By using

Algorithm 1: Fast-SCLF Decoding Algorithm

Input : \mathbf{y}, L, m, B

Output: $\hat{\mathbf{u}}$

```

1  $\beta \sim (0, 1)$  // Initialize  $\theta$ 
  /* FSCL Decoding with bit-flipping */
2  $\hat{\mathbf{u}}_{\text{init}}, \mathbf{Q}, \frac{\partial \mathbf{Q}}{\partial \theta} \leftarrow \text{InitialFSCL}(\mathbf{y}, \theta, L)$ 
  // Perform FSCL decoding with the reserved
  path-selection scheme
3 if  $\hat{\mathbf{u}}_{\text{init}}$  passes CRC then
4   return  $\hat{\mathbf{u}}_{\text{init}}$ 
5 else
6    $\{\iota_1^*, \dots, \iota_m^*\} \leftarrow \text{Sort}(\mathbf{Q})$ 
7   for  $i \leftarrow 1$  to  $m$  do
8      $\hat{\mathbf{u}}_{\text{flip}} \leftarrow \text{FSCL}(\mathbf{y}, \iota_i^*, L)$ 
9     if  $\hat{\mathbf{u}}_{\text{flip}}$  passes CRC then
10       $\theta \leftarrow \text{OptimizeTheta}(\theta, \iota_i^*, B, \mathbf{Q}, \frac{\partial \mathbf{Q}}{\partial \theta})$ 
11      return  $\hat{\mathbf{u}}_{\text{flip}}$ 
12 return  $\hat{\mathbf{u}}_{\text{init}}$ 

```

the chain rule and simple algebraic manipulations, given an instance \mathbf{Q} of a data sample d , $\frac{\partial \text{Loss}}{\partial \theta}$ can be calculated as

$$\frac{\partial \text{Loss}}{\partial \theta} = \sum_{k=1}^{K+C} \frac{\hat{o}_k - o_k}{(1 - \hat{o}_k) \exp(-Q_k)} \left[\frac{\partial \phi_k}{\partial \theta} - \hat{o}_k \sum_{j=1}^{K+C} \frac{\partial \phi_j}{\partial \theta} \right], \quad (37)$$

where $\phi_k = \exp(-Q_k)$ and $\frac{\partial \phi_k}{\partial \theta} = -\exp(-Q_k) \frac{\partial Q_k}{\partial \theta}$.

It can be observed that the computation of $\frac{\partial \text{Loss}}{\partial \theta}$ requires the computation of $\frac{\partial Q_k}{\partial \theta}$. Similar to Q_k , $\frac{\partial Q_k}{\partial \theta}$ can also be progressively calculated during the course of decoding. In particular, from (30) and (31) we obtain

$$\begin{aligned} \frac{\partial q_{k_l}}{\partial \theta} &= \frac{\partial q_{k-1_l}}{\partial \theta} + \frac{\partial \text{ReLU}(\theta - \gamma_{k_l})}{\partial \theta} \\ &= \frac{\partial q_{k-1_l}}{\partial \theta} + \mathbb{1}_{\theta > \gamma_{k_l}}, \end{aligned} \quad (38)$$

and

$$\frac{\partial q_{k_{\bar{l}}}}{\partial \theta} = \frac{\partial q_{k_l}}{\partial \theta} - 1, \quad (39)$$

respectively, and $\frac{\partial q_{0_l}}{\partial \theta} = 0 \forall l$. Since the values of $\frac{\partial q_{k_l}}{\partial \theta}$ and $\frac{\partial q_{k_{\bar{l}}}}{\partial \theta}$ are available for all the current active decoding paths with indices l and the forked paths with indices \bar{l} , after the path-metric sorting, $\frac{\partial Q_k}{\partial \theta}$ can be directly obtained as

$$\frac{\partial Q_k}{\partial \theta} = \frac{\partial q_{k_{l'_{\min}}}}{\partial \theta}. \quad (40)$$

Note that $\frac{\partial Q_k}{\partial \theta}$ contains integer values and $\frac{\partial Q_k}{\partial \theta} \in [-(K+C), K+C]$.

In Algorithm 1, we outline the proposed Fast-SCLF decoding algorithm integrated with the online training framework. The inputs of Algorithm 1 contain the channel vector \mathbf{y} , the list size L , the maximum number of additional FSCL decoding attempts m , and the size of the data batch \mathbb{D} denoted as B . The parameter θ is first randomly initialized from $(0, 1)$. Given a channel output vector \mathbf{y} , the initial FSCL decoding

Algorithm 2: Initial FSCL Decoding Algorithm

Input : \mathbf{y}, θ, L
Output: $\hat{\mathbf{u}}_{\text{init}}, \mathbf{Q}, \frac{\partial \mathbf{Q}}{\partial \theta}$

```

1 Function InitialFSCL( $\mathbf{y}, \theta, L$ ):
2   for each path-splitting with index  $k \in [1, K + C]$ 
3     do
4       Compute  $q_{k_l}$  and  $q_{k_{\tilde{l}}}$  based on (30) and (31)
5         for all the paths  $l$  and  $\tilde{l}$ 
6       Compute  $\frac{\partial q_{k_l}}{\partial \theta}$  and  $\frac{\partial q_{k_{\tilde{l}}}}{\partial \theta}$  based on (38) and (39)
7         for all the paths  $l$  and  $\tilde{l}$ 
8       Compute  $Q_k$  based on (32)
9       Compute  $\frac{\partial Q_k}{\partial \theta}$  based on (40)
10    for  $k \leftarrow 1$  to  $\log_2 L$  do
11       $Q_k \leftarrow \infty$ 
12       $\frac{\partial Q_k}{\partial \theta} \leftarrow 0$ 
13    Obtain  $\hat{\mathbf{u}}_{\text{init}}$  from the first FSCL decoding attempt
14  return  $\hat{\mathbf{u}}_{\text{init}}, \mathbf{Q}, \frac{\partial \mathbf{Q}}{\partial \theta}$ 

```

Algorithm 3: Parameter optimization

Input : $\theta, \nu_e, B, \mathbf{Q}, \frac{\partial \mathbf{Q}}{\partial \theta}$
Output: θ

```

1  $c \leftarrow 0$  // The number of data samples used
2  $\Delta \leftarrow 0$  // The accumulated gradient
3 Function OptimizeTheta( $\theta, \nu_e, B, \mathbf{Q}, \frac{\partial \mathbf{Q}}{\partial \theta}$ ):
4   /* Optimization of  $\theta$  */
5    $c \leftarrow c + 1$  // Increase the number of sample
6   Construct  $\sigma$  using (33) given  $\nu_e$ 
7   Compute  $\hat{\sigma}$  using (34) given  $\mathbf{Q}$ 
8   Compute  $\frac{\partial \text{Loss}}{\partial \theta}$  using (37) given  $\mathbf{Q}$  and  $\frac{\partial \mathbf{Q}}{\partial \theta}$ 
9    $\Delta \leftarrow \Delta + \frac{\partial \text{Loss}}{\partial \theta}$  // Accumulate the gradient
10  if  $c \bmod B == 0$  then
11     $\theta \leftarrow \theta - \sigma \frac{\Delta}{B}$  // Update the parameter
12     $\Delta \leftarrow 0$  // Reset the gradient
13  return  $\theta$ 

```

is carried out in the InitialFSCL(\cdot) function described in Algorithm 2, which performs the conventional FSCL decoding operations to obtain the estimated message word $\hat{\mathbf{u}}_{\text{init}}$. In addition, at each path splitting with index k of the initial FSCL decoding attempt, the path-error metrics $\{q_{k_l}, q_{k_{\tilde{l}}}\}$ and the derivatives $\{\frac{\partial q_{k_l}}{\partial \theta}, \frac{\partial q_{k_{\tilde{l}}}}{\partial \theta}\}$ of all the paths with indices l and \tilde{l} are progressively calculated (line 3-4, Algorithm 1), followed by the computations of Q_k and $\frac{\partial Q_k}{\partial \theta}$ (line 5-6, Algorithm 1). Note that $\frac{\partial Q_k}{\partial \theta}$ is set to 0 and Q_k is set to ∞ for all the path splittings with index $k \in [1, \log_2 L]$. At the end of the InitialFSCL(\cdot) function, the first estimate of the message word $\hat{\mathbf{u}}_{\text{init}}$, the path-selection error metrics \mathbf{Q} , and their derivatives $\frac{\partial \mathbf{Q}}{\partial \theta}$ are returned to the main decoding algorithm.

In the next step, if $\hat{\mathbf{u}}_{\text{init}}$ satisfies the CRC test, the Fast-SCLF decoder then outputs $\hat{\mathbf{u}}_{\text{init}}$ and terminates. Otherwise, the path-

selection error metrics \mathbf{Q} are sorted in the increasing order such that $Q_{i_1^*} \leq \dots \leq Q_{i_{K+C}^*}$, and the path-splitting indices corresponding to the m smallest elements of \mathbf{Q} are selected for the secondary FSCL decoding attempts, i.e., $\{i_1^*, \dots, i_m^*\}$. The Fast-SCLF decoder then performs a maximum number of m additional FSCL decoding attempts (line 7, Algorithm 1) with each attempt performs the reversed path-selection scheme at a different path-flipping index i_i^* . If one of the secondary FSCL decoding attempts results in a successful CRC verification, the optimization process of θ implemented in the OptimizeTheta(\cdot) function is queried, which performs the proposed optimization process based on supervised learning. The details of the function OptimizeTheta(\cdot) are provided in Algorithm 3. To reduce the memory consumption required to store the data batch \mathbb{D} for each parameter update, we use a variable Δ in Algorithm 3 to store the accumulated gradients $\sum_{\forall d \in \mathbb{D}} \frac{\partial \text{Loss}}{\partial \theta}$ as shown in (36). In addition, each data sample d is completely different from the others due to the presence of channel noise. Therefore, the proposed training framework can prevent overfitting without the need of using a separate validation set, which also reduces the memory consumption of the parameter optimization.

Finally, if the resulting estimated message word $\hat{\mathbf{u}}_{\text{flip}}$ obtained from one of the secondary FSCL decoding attempts satisfies the CRC test, $\hat{\mathbf{u}}_{\text{flip}}$ is returned as the final decoding output. On the other hand, if none of the secondary FSCL decoding attempt can provide a message word that passes the CRC verification, the estimated message word $\hat{\mathbf{u}}_{\text{init}}$ of the initial FSCL decoding is returned as the final output of the decoding process.

C. Quantitative Complexity Analysis

To quantify the computational complexity of the decoders considered in this paper, we count the number of floating-point additions/subtractions and floating-point comparisons performed. In this paper, we use the merge sort algorithm to sort a vector with N elements, which requires a worst case of $N \lceil \log_2 N \rceil - 2^{\lceil \log_2 N \rceil} + 1$ floating-point comparisons if N is not a power of 2, otherwise the number of comparisons needed is $N \log_2 N$ [18, Chapter 2].

We compute the decoding latency of the SCL-based decoders by using the method considered in [9], [10]. In particular, we count the number of time steps for various decoding operations with the following assumptions. First, we assume that there is no resource constrain, therefore all the operations that can be computed concurrently require one time step [9], [10]. Second, the hard decisions obtained from the LLR values and binary operations are computed instantaneously [5], [9], [10]. Finally, we consider the time steps required by a merge sort algorithm to sort a vector of size N is $\lceil \log_2 N \rceil$.

Note that in practice the OptimizeTheta(\cdot) function can be implemented using a general-purpose microprocessor while the rest of the proposed Fast-SCLF decoder can be implemented in hardware. This is because the OptimizeTheta(\cdot) function requires costly transcendental computations which are not hardware friendly. Instead, the Fast-SCLF decoder reads the parameter θ from memory when a new value of θ

is updated by the `OptimizeTheta(·)` function. Therefore, we do not include the computational complexity, decoding latency, and memory requirement of the `OptimizeTheta(·)` function when analyzing the proposed Fast-SCLF decoder. Based on this assumption, the Fast-SCLF decoder needs to store the parameter θ , the bit-index ι_e , the path-selection error metrics \mathbf{Q} and the derivatives $\frac{\partial \mathbf{Q}}{\partial \theta}$ to memory, which are required by the `OptimizeTheta(·)` function. Therefore, the memory consumption of the proposed decoder with list size L can be calculated as

$$\begin{aligned} \mathcal{M}_{\text{Fast-SCLF}} &= \mathcal{M}_{\text{FSCL}} + \underbrace{b_f}_{\theta\text{-memory}} + \underbrace{Lb_f}_{q\text{-memory}} + \underbrace{Lb_i}_{\frac{\partial q}{\partial \theta}\text{-memory}} \\ &+ \underbrace{\lceil \log_2(K+C) \rceil}_{\iota_e\text{-memory}} + \underbrace{(K+C)b_f}_{\mathbf{Q}\text{-memory}} + \underbrace{(K+C)b_i}_{\frac{\partial \mathbf{Q}}{\partial \theta}\text{-memory}} \\ &= \mathcal{M}_{\text{FSCL}} + (K+C+L+1)b_f + (K+C)b_i \\ &+ \lceil \log_2(K+C) \rceil. \end{aligned} \quad (41)$$

where b_i is the number of memory bits used to quantize the integer values of $\frac{\partial \mathbf{Q}}{\partial \theta}$ and $\frac{\partial q}{\partial \theta}$. In this paper, we quantize an integer number a by using the sign-magnitude representation, which requires $\lceil \log_2(|a|) \rceil + 1$ memory bits.

IV. EVALUATION

A. Optimized Parameter and Error-Correction Performance

We measure the accuracy of the proposed training framework by calculating the expected probability that the most probable error index ι derived from (28) is the actual error index ι_e^* given that the initial FSCL decoding attempt does not satisfy the CRC test. The training accuracy is computed as

$$\mathbb{E}[\text{Pr}(\iota = \iota_e^* | \mathbf{y})] = \frac{\sum_{\forall \iota} \mathbb{1}_{\iota = \iota_e^*}}{\# \text{ training samples used}}. \quad (42)$$

In this paper, we use Adam [19] as the SGD variant with $\sigma = 0.005$ and $B = 100$. In addition, we set $b_f = 32$ for both the training and decoding processes of the proposed decoder. Fig. 6 illustrates the learning curves of θ for $\mathcal{P}(512, 256)$ and $\mathcal{P}(512, 384)$ with $m = 80$, $L = 32$, and $b_i = \{\lceil \log_2(K+C) \rceil + 1, 2\}$. The polar codes are concatenated with the 24-bit CRC used in 5G. Note that with $b_i = \lceil \log_2(K+C) \rceil + 1$ the maximum and minimum values of the derivatives $\frac{\partial \mathbf{Q}}{\partial \theta}$ and $\frac{\partial q}{\partial \theta}$ are exactly represented under the sign-magnitude quantization scheme. On the other hand with $b_i = 2$, $\frac{\partial \mathbf{Q}}{\partial \theta}$ and $\frac{\partial q}{\partial \theta}$ are constrained to $\{-1, 0, 1\}$. As observed from Fig. 6, constraining $\frac{\partial \mathbf{Q}}{\partial \theta}$ and $\frac{\partial q}{\partial \theta}$ with the ternary values of $\{-1, 0, 1\}$ does not significantly degrade the estimation accuracy of the proposed error model, while reducing the memory requirement of the Fast-SCLF decoder as b_i is reduced from $\lceil \log_2(K+C) \rceil + 1$ to 2 (see (41)). Therefore, in the rest of this paper, we use $b_i = 2$ when considering the proposed Fast-SCLF decoding algorithm.

Fig. 7 shows the error correction performance in terms of FER of the SCLF-based decoders where $m = 50$ for $L \in \{2, 4, 8\}$ and $m = 80$ for $L \in \{16, 32\}$. The proposed decoder is denoted as Fast-SCLF- L - m while the SCLF decoder is denoted as SCLF- L - m . In addition, the FER curves of the

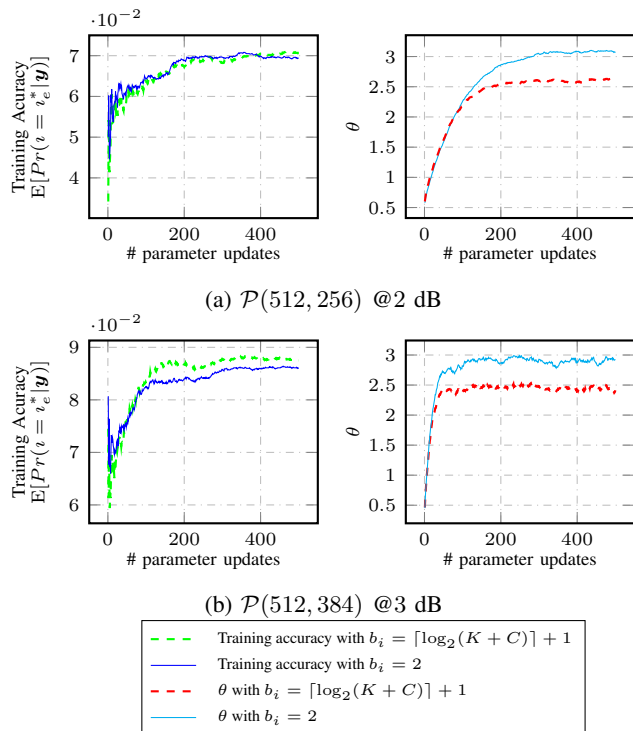


Fig. 6: Training curves of the parameter θ for $\mathcal{P}(512, 256)$ and $\mathcal{P}(512, 384)$ with $L = 32$ and $m = 80$. A 24-bit CRC used in 5G is concatenated with the polar codes.

FSCL decoder with list size 32 is also plotted for comparison. We consider $\mathcal{P}(512, 256)$ and $\mathcal{P}(512, 384)$ used in Fig. 5, and the 24-bit CRC used in 5G is concatenated with the polar codes. The parameter θ used in (19) of the SCLF decoder is optimized offline for each value of L with the Monte-Carlo approach [14]. The E_b/N_0 values of the Monte-Carlo simulations are chosen to have an FER of approximately 10^{-4} with the selected values of L and m . From Fig. 7, it can be observed that under all settings the SCLF decoder has a relatively similar error-correction performance compared to that of the proposed Fast-SCLF decoder. In some configurations of the polar codes, the Fast-SCLF decoder obtains a small FER gain over the SCLF decoder with the same list size. This is because in many instances of the channel output \mathbf{y} , reversing an error decision at the parent-node level results in the corrections of more than one information bits located at the leaf-node level of the same parent node. This behavior is also observed for the case of the ideal Fast-SCLF decoder presented in Section III-A.

B. Computational Complexity, Decoding Latency, and Memory Requirement

In Table I, we summarize the average computational complexities (\mathcal{C}) and the average decoding latency (\mathcal{L}) of the SCLF-based decoders with the numerical analysis approach considered in this paper. The E_b/N_0 values in Table I are selected from Fig. 7 where the simulated FER values of the SCLF-based decoder are closest to the target FER of 10^{-4} . In addition, the savings of the Fast-SCLF decoder in

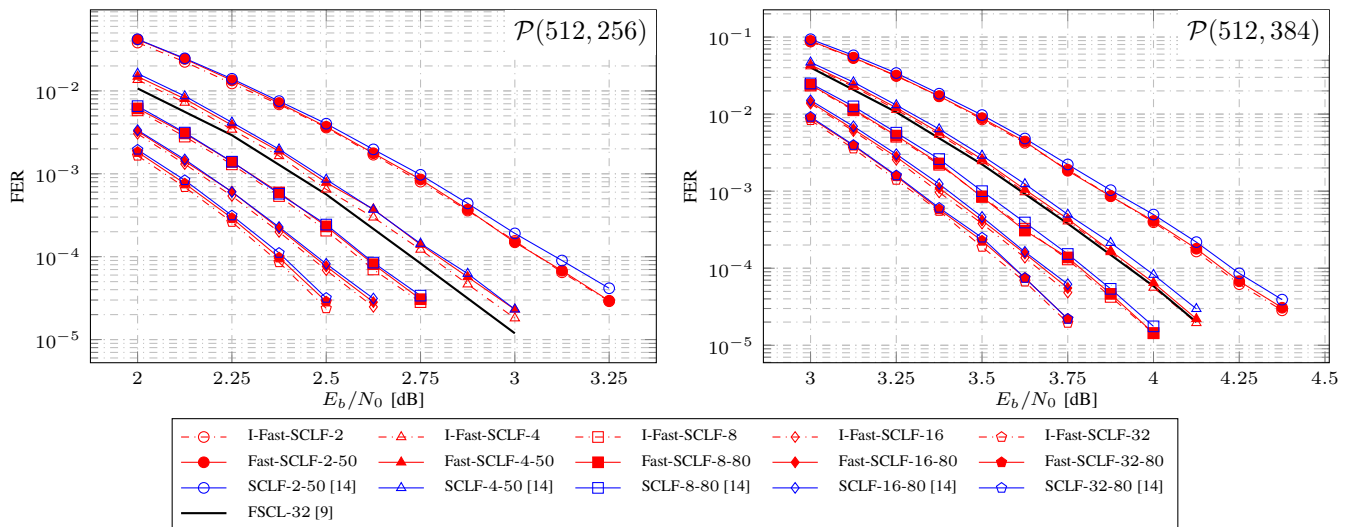


Fig. 7: Error-correction performance of all the SCLF-based decoders considered in this paper. The FER values of the FSCL decoder with list size $L = 32$ is also plotted for comparison.

TABLE I: Summary of the average computational complexity in terms of the number of additions/subtractions and comparisons performed (\mathcal{C}) and the average decoding latency in time steps (\mathcal{L}) of the SCLF-based decoding algorithms for $\mathcal{P}(512, 256)$ and $\mathcal{P}(512, 384)$ considered in Fig. 7.

$\mathcal{P}(512, 256)$	$L = 2, m = 50$ @3.0 dB		$L = 4, m = 50$ @2.75 dB		$L = 8, m = 80$ @2.625 dB		$L = 16, m = 80$ @2.5 dB		$L = 32, m = 80$ @2.375 dB	
	\mathcal{C}	\mathcal{L}	\mathcal{C}	\mathcal{L}	\mathcal{C}	\mathcal{L}	\mathcal{C}	\mathcal{L}	\mathcal{C}	\mathcal{L}
SCLF	1.48E+4	1.88E+3	2.69E+4	2.17E+3	5.21E+4	2.44E+3	1.13E+5	2.72E+3	2.21E+5	3.02E+3
Fast-SCLF	1.40E+4	5.01E+2	2.67E+4	7.88E+2	5.47E+4	1.06E+3	1.23E+5	1.34E+3	3.01E+5	1.63E+3
Saving	4.7%	73.4%	0.7%	63.7%	-5.0%	56.6%	-8.8%	50.7%	-36.2%	46.0%

$\mathcal{P}(512, 384)$	$L = 2, m = 50$ @4.25 dB		$L = 4, m = 50$ @4.0 dB		$L = 8, m = 80$ @3.75 dB		$L = 16, m = 80$ @3.75 dB		$L = 32, m = 80$ @3.625 dB	
	\mathcal{C}	\mathcal{L}	\mathcal{C}	\mathcal{L}	\mathcal{C}	\mathcal{L}	\mathcal{C}	\mathcal{L}	\mathcal{C}	\mathcal{L}
SCLF	1.71E+4	1.97E+3	3.18E+4	2.40E+3	6.36E+4	2.87E+3	1.28E+5	3.23E+3	2.68E+5	3.65E+3
Fast-SCLF	1.74E+4	5.73E+2	3.21E+4	9.90E+2	6.77E+4	1.43E+3	1.42E+5	1.80E+3	3.14E+5	2.25E+3
Saving	-1.7%	70.9%	-0.9%	58.8%	-6.4%	50.0%	-13.6%	43.8%	-54.0%	38.4%

terms of the complexity and latency with respect to those of the SCLF decoder are also provided in Table I. The effectiveness of the proposed decoder is confirmed in Table I as the decoding latency of the SCLF decoding algorithm is significantly higher than that of the Fast-SCLF decoder with the same list size. However, with the list size increases the Fast-SCLF decoder imposes a more significant computational complexity overhead when compared to that of the SCLF decoder. This is due to the complexity devoted for sorting the LLR values associated with the special SPC and Rate-1 nodes, which significantly increases with the increase of the list size under FSCL decoding.

Note that the path-selection error metric of SCLF decoding can be progressively calculated using a similar approach as described in (30) and (31). Therefore, the memory consumption of the SCLF decoder with list size L is calculated as

$$\begin{aligned} \mathcal{M}_{\text{SCLF}} &= \mathcal{M}_{\text{SCL}} + \underbrace{b_f}_{\theta\text{-memory}} + \underbrace{Lb_f}_{q\text{-memory}} + \underbrace{(K+C)b_f}_{Q\text{-memory}} \\ &= \mathcal{M}_{\text{SCL}} + (K+C+L+1)b_f. \end{aligned} \quad (43)$$

In Table II, we summarize the memory consumption of all the

TABLE II: Memory requirement in KBits of the SCL-based decoders considered in this paper.

$\mathcal{P}(512, 256)$	L				
	2	4	8	16	32
SCL [5], FSCL [9]	50.0	84.0	152.0	288.0	560.0
SCLF [14]	58.8	92.9	161.0	297.3	569.8
Fast-SCLF [proposed]	59.4	93.5	161.6	297.8	570.3

$\mathcal{P}(512, 384)$	L				
	2	4	8	16	32
SCL [5], FSCL [9]	50.0	84.0	152.0	288.0	560.0
SCLF [14]	62.8	97.0	165.0	301.3	573.8
Fast-SCLF [proposed]	63.6	97.7	165.8	302.1	574.6

SCL-based decoders in this paper.

As observed from Fig. 7, the error-correction performance of the SCLF and Fast-SCLF decoders with $L = 4$ and $m = 50$ is within a 0.1 dB gap when compared with the FER performance of the FSCL-32 decoder at all the considered SNR values. Therefore, in Fig. 8 we illustrate the average complexity and decoding latency of the FSCL-32, SCLF-4-50

TABLE III: The average computational complexity, average decoding latency, memory consumption, and error-correction performance degradation of the Fast-SCLF and SCLF decoders with list size 4 in comparison with those of the FSCL-32 decoder.

	$\mathcal{P}(512, 256)$ @2.75 dB			$\mathcal{P}(512, 384)$ @4.0 dB		
	Fast-SCLF-4	SCLF-4	FSCL-32	Fast-SCLF-4	SCLF-4	FSCL-32
\mathcal{C} (# operations)	2.67E+4	2.69E+4	2.46E+5	3.21E+4	3.18E+4	2.12E+5
\mathcal{L} (time-steps)	7.88E+2	2.17E+3	1.40E+3	9.90E+2	2.40E+3	1.36E+3
\mathcal{M} (KBits)	93.5	92.9	560.0	97.7	97.0	560.0
FER Performance Degradation (dB)	0.07	0.07	-	0.02	0.05	-

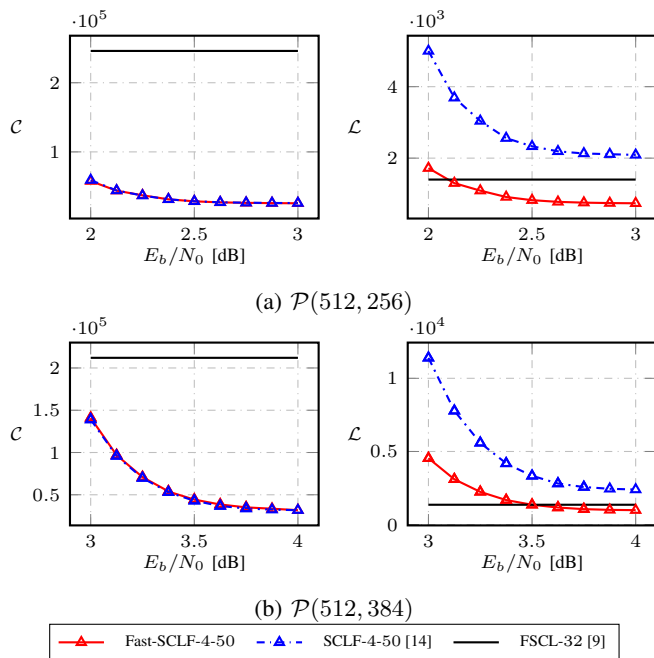


Fig. 8: Average computational complexity and average latency of the SCLF-based decoders with list size 4 and the FSCL decoder with list size 32.

and Fast-SCLF-4-50 decoders, whose FER values are plotted in Fig. 7. As seen from Fig. 8, the SCLF-based decoders with list size 4 have a relatively similar computational complexity and are greatly smaller than that of the FSCL-32 decoder, especially at the high SNR regimes. Furthermore, the average decoding latency of the proposed Fast-SCLF-4-50 decoder is significantly smaller than those of the FSCL-32 and SCLF-4-50 decoder at the high SNR regimes. In Table III, we summarize the error-correction performance degradation, the average computational complexity, memory requirement, and average decoding latency of the SCLF-based decoders with list size 4 and those of the FSCL-32 decoder at $E_b/N_0 = 2.75$ dB for $\mathcal{P}(512, 256)$ and at $E_b/N_0 = 4.0$ dB for $\mathcal{P}(512, 384)$. Note that the E_b/N_0 values are selected to allow an FER performance close to the target FER of 10^{-4} for the SCLF-based decoders. In particular, at $E_b/N_0 = 2.75$ dB for $\mathcal{P}(512, 256)$, the average complexity and average latency of the Fast-SCLF-4-50 decoder account for approximately 11% and 56% of the complexity and latency of the FSCL-32 decoder, respectively. In addition, at $E_b/N_0 = 4.0$ dB and for $\mathcal{P}(512, 384)$, the Fast-SCLF-4-50 decoder reduces 85%

of the average complexity and 27% of the average latency, also compared with the FSCL-32 decoder. The SCLF-based decoders with list size 4 only consume around 17% of the memory requirement of the FSCL-32 decoder, while incurring up to 0.07 dB degradation in the error-correction performance compared to FSCL-32.

V. CONCLUSION

In this paper, we proposed a bit-flipping scheme tailored to the state-of-the-art fast successive-cancellation list (FSCL) decoding, forming the fast successive-cancellation list flip decoder (Fast-SCLF). We then derived a parameterized path-selection error metric that estimates the erroneous path-splitting index at which the correct decoding path is eliminated from the initial FSCL decoding. The trainable parameter of the proposed error model is optimized using online supervised learning, which automatically trains the parameter at the operating signal-to-noise ratio of the decoder without the need of pilot signals. We numerically evaluated the proposed decoding algorithm and compared its error-correction performance, average computational complexity, average decoding latency, and memory requirement with those of the state-of-the-art FSCL decoder and successive-cancellation list flip (SCLF) decoder. The simulation results confirm the effectiveness of the proposed decoder when compared with the FSCL and the SCLF decoders for different polar codes and various list sizes.

REFERENCES

- [1] E. Arkan, "Channel polarization: A method for constructing capacity-achieving codes for symmetric binary-input memoryless channels," *IEEE Trans. Inf. Theory*, vol. 55, no. 7, pp. 3051–3073, July 2009.
- [2] 3GPP, "Multiplexing and channel coding (Release 10) 3GPP TS 21.101 v10.4.0." Oct. 2018. [Online]. Available: http://www.3gpp.org/ftp/Specs/2018-09/Rel-10/21_series/21101-a40.zip
- [3] I. Tal and A. Vardy, "List decoding of polar codes," *IEEE Trans. Inf. Theory*, vol. 61, no. 5, pp. 2213–2226, March 2015.
- [4] K. Niu and K. Chen, "CRC-aided decoding of polar codes," *IEEE Commun. Lett.*, vol. 16, no. 10, pp. 1668–1671, 2012.
- [5] A. Balatsoukas-Stimming, M. B. Parizi, and A. Burg, "LLR-based successive cancellation list decoding of polar codes," *IEEE Trans. Signal Process.*, vol. 63, no. 19, pp. 5165–5179, Oct. 2015.
- [6] A. Alamdar-Yazdi and F. R. Kschischang, "A simplified successive-cancellation decoder for polar codes," *IEEE Commun. Lett.*, vol. 15, no. 12, pp. 1378–1380, October 2011.
- [7] G. Sarkis, P. Giard, A. Vardy, C. Thibault, and W. J. Gross, "Fast polar decoders: Algorithm and implementation," *IEEE J. Sel. Areas Commun.*, vol. 32, no. 5, pp. 946–957, April 2014.
- [8] S. A. Hashemi, C. Condo, and W. J. Gross, "A fast polar code list decoder architecture based on sphere decoding," *IEEE Trans. on Circuits and Sys. I*, vol. 63, no. 12, pp. 2368–2380, Dec 2016.

- [9] —, “Fast and flexible successive-cancellation list decoders for polar codes,” *IEEE Trans. on Sig. Proc.*, vol. 65, no. 21, pp. 5756–5769, Nov 2017.
- [10] M. H. Ardakani, M. Hanif, M. Ardakani, and C. Tellambura, “Fast successive-cancellation-based decoders of polar codes,” *IEEE Trans. Commun.*, vol. 67, no. 7, pp. 4562–4574, 2019.
- [11] M. Hanif, M. H. Ardakani, and M. Ardakani, “Fast list decoding of polar codes: Decoders for additional nodes,” in *IEEE Wire. Comm. and Net. Conf. Work.*, April 2018, pp. 37–42.
- [12] S. A. Hashemi, C. Condo, F. Ercan, and W. J. Gross, “Memory-efficient polar decoders,” *IEEE J. Emerg. Sel. Topics Circuits Syst.*, vol. 7, no. 4, pp. 604–615, Dec. 2017.
- [13] S. A. Hashemi, N. Doan, T. Tonnellier, and W. J. Gross, “Deep-learning-aided successive-cancellation decoding of polar codes,” in *53rd Asilomar Conf. on Sig., Sys., and Comp.*, 2019, pp. 532–536.
- [14] F. Cheng, A. Liu, Y. Zhang, and J. Ren, “Bit-flip algorithm for successive cancellation list decoder of polar codes,” *IEEE Access*, vol. 7, pp. 58 346–58 352, 2019.
- [15] L. Chandesris, V. Savin, and D. Declercq, “Dynamic-SCFlip decoding of polar codes,” *IEEE Trans. Commun.*, vol. 66, no. 6, pp. 2333–2345, June 2018.
- [16] F. Ercan, T. Tonnellier, N. Doan, and W. J. Gross, “Practical dynamic SC-flip polar decoders: Algorithm and implementation,” *IEEE Trans. Signal Process.*, vol. 68, pp. 5441–5456, 2020.
- [17] N. Doan, S. A. Hashemi, F. Ercan, T. Tonnellier, and W. J. Gross, “Neural successive cancellation flip decoding of polar codes,” *J. Sig. Proc. Sys.*, pp. 1–12, 2020.
- [18] T. H. Cormen, C. E. Leiserson, R. L. Rivest, and C. Stein, “Introduction to algorithms.” MIT press, 2009.
- [19] D. P. Kingma and J. Ba, “Adam: A method for stochastic optimization,” *arXiv preprint arXiv:1412.6980*, 2014.